

Journal Pre-proofs

Nitrogen-fixing of ultrasmall Pd-Based bimetallic nanoclusters on carbon supports

Lei Wang, Peng Yin, Le-Le Zhang, Shan-Cheng Shen, Shi-Long Xu, Ping Chen, Hai-Wei Liang

PII: S0021-9517(20)30233-5
DOI: <https://doi.org/10.1016/j.jcat.2020.06.003>
Reference: YJCAT 13774

To appear in: *Journal of Catalysis*

Received Date: 7 January 2020
Revised Date: 26 May 2020
Accepted Date: 2 June 2020

Please cite this article as: L. Wang, P. Yin, L-L. Zhang, S-C. Shen, S-L. Xu, P. Chen, H-W. Liang, Nitrogen-fixing of ultrasmall Pd-Based bimetallic nanoclusters on carbon supports, *Journal of Catalysis* (2020), doi: <https://doi.org/10.1016/j.jcat.2020.06.003>

This is a PDF file of an article that has undergone enhancements after acceptance, such as the addition of a cover page and metadata, and formatting for readability, but it is not yet the definitive version of record. This version will undergo additional copyediting, typesetting and review before it is published in its final form, but we are providing this version to give early visibility of the article. Please note that, during the production process, errors may be discovered which could affect the content, and all legal disclaimers that apply to the journal pertain.

© 2020 Elsevier Inc. All rights reserved.



Nitrogen-fixing of ultrasmall Pd-Based bimetallic nanoclusters on carbon supports

Lei Wang^a, Peng Yin^a, Le-Le Zhang^a, Shan-Cheng Shen^a, Shi-Long Xu^a, Ping Chen^b, Hai-Wei Liang^{a,*}

^a Division of Nanomaterials & Chemistry, Hefei National Laboratory for Physical Sciences at the Microscale, Department of Chemistry, University of Science and Technology of China, Hefei, 230026, China.

^b School of Chemistry and Chemical Engineering, Anhui University, Hefei, Anhui 230601, China.

*Corresponding author. E-mail address: hwliang@ustc.edu.cn (H.-W. Liang)

Keywords: Nitrogen-fixing strategy, Ultrasmall Pd-based alloys, Alkynes semihydrogenation reaction

ABSTRACT: Synthesis of supported Pd-based bimetallic catalysts is of great importance in the heterogeneous catalysis field owing to their optimal geometric and electronic effects. Downsizing active metals to ultrasmall nanocluster (< 2 nm), which is mandatory for maximizing the metal atom utilization, however remains as formidable synthesis challenges. Here, we present a general synthetic approach to sub-2 nm Pd-based bimetallic nanoclusters on porous nitrogen-doped carbon supports, in which the strong chemical interaction between metal and nitrogen largely suppresses the metal aggregation during the H₂-reduction at 400~500 °C. Through the nitrogen-fixing strategy, we prepare 9 sub-2 nm Pd-based bimetallic nanocluster catalysts by conventional impregnation process. The prepared supported bimetallic Pd-Pb nanocluster catalyst exhibit a high turnover frequency of 1092 hour⁻¹ for the semihydrogenation of phenylacetylene under a mild condition (30 °C, 5 bar H₂), along with a high selectivity of $>93\%$ to styrene, demonstrating the alloying and small-size effects in the bimetallic nanocluster catalysts.

1. Introduction

Supported Pd-based catalysts have attracted immense interests in both industrial and fundamental researches over the last decades, owing to their distinct catalytic properties in diverse important reactions, such as hydrogenation [1-3] and dehydrogenation [4, 5], electrocatalytic reaction [6, 7], methane oxidation [8], CO oxidation [9, 10], C-H activation [11] and organic coupling reactions [12]. By alloying Pd with foreign metal atoms (including noble and non-noble metal), the catalytic performance could be flexibly regulated via changing the geometric construction, coordination environment and electronic properties of the catalysts [13-18]. On the other hand, downsizing metal to the nanometer scale is mandatory for increasing their specific surface areas and thus their activity

normalized to mass; the optimum particle size of <2 nm is required for maximizing the metal atom utilization. Meanwhile, the electronic properties of metals are also highly dependent on the particle size particularly below 2 nm, due to the quantum size effects and surface effects [19-22].

The synthetic challenge of supported ultrasmall nanoclusters lies in their inherent thermodynamic instability, as metal species tend to aggregate into larger particles due to the sharply increased surface free energy with the decrease of particle size. Such intrinsic drawback makes it highly challenging to prepare ultrasmall nanoclusters by conventional impregnation process, even with high-surface-area supports. To this end, some emerging strategies have been developed recently for meeting the synthesis challenges for ultrasmall bimetallic nanocluster catalysts, typically including: 1) colloidal synthesis with organic capping agents [23], 2) nanoconfinement synthesis with zeolites [24, 25], or metal-organic framework [26-29] as carriers, and 3) organometallic precursor methods [30, 31]. Nevertheless, the organic capping agents or porous carriers around the bimetallic nanoclusters often block the active metal surface or significantly increase the mass-transport resistance during the catalysis [32-34]. Although the direct thermal decomposition of hetero-bimetallic organometallic compounds could produce alloyed nanoclusters with atomic-scale control, the high cost of the organometallic precursors hampers the scalable synthesis for practical applications [35]. Very recently, two promising methods, that is, strong electrostatic adsorption [36] and surface inorganometallic chemistry [37] were reported for the general synthesis of ultrasmall nanoclusters on silica supports. In these works, the positively charged metal-amine complexes were used as precursors that could electrostatically interact with the negatively charged silica supports, which facilitated the homogeneous adsorption of metal precursors on silica and eventually guaranteed the formation of alloyed nanoclusters. The limited commercial availability of the metal-amine complexes probably

restricts the compositional variation of the bimetallic nanocluster catalysts.

Here, we demonstrate a facile and general nitrogen-fixing strategy to prepare a family of sub-2 nm Pd-based bimetallic nanoclusters with porous nitrogen-doped carbon (N-C) as supports. The strong chemical interaction between nitrogen and anchored metal species largely suppresses the metal aggregation during H₂ reduction at 400~500 °C. Such strong nitrogen-fixing ability for metals allows us to prepare 9 sub-2 nm Pd-based bimetallic nanocluster catalysts by conventional impregnation process with common metal precursors (**Fig. 1**). The prepared Pd-Pb/N-C catalyst displays superior activity and selectivity towards the semihydrogenation reaction of a wide range of terminal alkynes. Although the N- [32, 38, 39] and S-doped carbons [40, 41] have been used as supports for the synthesis of ultrafine monometallic nanoclusters and even atomically dispersed metals, there are few reports yet on the synthesis of ultrasmall bimetallic nanoparticles of < 2 nm on carbons.

2. Experimental

2.1. Material

Hexaketocyclohexane octahydrate was purchased from Shanghai Jiangge Chem Co. Ltd. Pd/C (5 wt%) was purchased from Shanghai URChem Ltd. All the alkyne reagents were purchased from Aladdin Co. Ltd.. All other chemicals were purchased from Sinopharm Chemical Reagent Co. Ltd., China. All the chemicals were used as received without further purification.

2.2. Synthesis of the N-C support

The N-C support was synthesized by the reported molten salt (ZnCl₂) method [42]. In a typical synthesis, 2.5 g of hexaketocyclohexane octahydrate, 1.44 g of urea and 10.0 g of ZnCl₂ were mixed together and ground in an agate mortar. The mixture was transferred into a quartz boat and heated to

100 °C for 1 hour to form a class of eutectic mixture. Then, the eutectic mixture was further heated to 600 °C for 3 h under flowing nitrogen atmosphere with a heating rate of 2.5 °C min⁻¹. After cooling to room temperature, the resultant solids underwent acid etching with 0.5 M HCl at 80 °C for 6 hours. The product was collected by filtration and washed thoroughly with deionized water and dried at 85 °C for 12 hours under vacuum. The low-nitrogen-content carbon support (LN-C) support was obtained by the high-temperature treatment of the as-prepared N-C in 5 vol% H₂/Ar at 1100 °C for 2 hours.

2.3. Synthesis of the bimetallic nanocluster catalysts

The bimetallic nanocluster catalysts were prepared by the conventional impregnation method. Taking the synthesis of Pd-Pb/N-C (Pd/Pb=1:2) catalyst for example, 50 mg of N-C was first dispersed into 20 mL of deionized water before a certain of palladium chloride in hydrochloric acid solution (1.25 mg Pd) and lead nitrate solution (4.87 mg Pb) were added. After ultrasonic treatment for 1 hour and vigorous stirring for 12 hours, the water in the mixture was removed by rotary evaporation. Finally, the metal salt/N-C precursors were treated in following 5 vol% H₂/Ar for 2 hours at 500 °C with a heating rate of 5 °C min⁻¹. Other Pd bimetallic nanocluster catalysts were also prepared by similar process. The detailed synthesis recipes for all the catalysts were summarized in Table S1.

2.4. Physicochemical characterizations

Low magnification high-angle annular dark-field scanning transmission electron microscopy (HAADF-STEM) images were obtained on FEI Talos F200X operated at 200 kV. Atomic resolution HAADF-STEM images were obtained on probe aberration-corrected JEM-ARM200F with accelerating voltage of 200 kV. Energy-dispersive X-ray spectroscopy (EDS) mappings and line scan were carried out on FEI Talos F200X, equipped with Super X-EDS system (four systematically arranged windowless silicon drift detectors) at 200 kV. Powder X-ray diffraction (XRD) analysis was

performed on a Philips X'Pert PRO SUPER X-ray diffractometer with Cu K α radiation ($\lambda=1.54056$ Å). The operation voltage and current were 40 kV and 150 mA, and the scan speed was set at 1.2°min^{-1} with 2θ range of $10\text{--}90^\circ$. The surface chemical state of the Pd species were analyzed by X-ray photoelectron spectroscopy (XPS) conducted on Emeco_S-CAL MKII with an excitation source of Mg K α radiation (1253.6 eV). All the spectra were calibrated with respect to the C 1s peak at 284.8 eV. The Brunauer–Emmett–Teller (BET) surface areas and pore size distribution of the supports were measured by N₂ sorption isotherms (77 K) and nonlinear density functional theory model with ASAP 2020 (*Micromeritics*). Elemental analysis of N and O in NC support were determined with an Elementar Vario EL elemental analyzer. The metal content in N-C was conducted on a Varian 710-ES (Agilent Technologies) inductively coupled plasma atomic emission spectrometry (ICP-AES) instrument after digestion in aqua regia overnight at 373 K. The X-ray absorption fine structure (XAFS) spectra at the Pd k-edge were measured in fluorescence mode at the BL14W1 station of Shanghai Synchrotron Radiation Facility (SSRF) operated at 3.5 GeV and 220 mA. The X-ray energy was tuned by a fix-exit Si (111) double crystal monochromator and calibrated using Pd foil before the experiments. All samples were pelletized as disks with a diameter of 8 mm and a thickness of ~ 2 mm. The raw data analyses were conducted by using Athena program in IFEFFIT software package. The energy was first calibrated, then the pre-edge background of spectrum was subtracted and post-edge was normalized. The k range for Fourier transformation was from 2.5 to 12.4 \AA^{-1} to obtain a radial distribution function.

2.5. Hydrogenation of phenylacetylene

In a typical catalysis experiment, 110 μL of phenylacetylene (1 mmol), a certain amount of Pd-Pb/N-C (Pd/Pb=1:2) catalyst, and 1 mL of ethanol were added into a glass reaction vessel. Next, the reaction vessel was placed into an autoclave reactor, subsequently purged with H₂ for five times, and pressurized to 5 bar H₂. The reactor was preheated to 30°C and then stirred at 1000 rpm for a certain

time. Finally, the reaction products were analyzed using a Shimadzu gas chromatograph with a flame ionization detector and with high-purity nitrogen as the carrier gas. The TOF for hydrogenation of phenylacetylene was calculated under the conversion of 15-30% based on the total amount of Pd. For the recycling experiments, the catalyst was separated by centrifugation, washed with ethanol and ethyl acetate for several times, and then dried under vacuum condition at 60 °C overnight.

3. Results and discussion

3.1. Synthesis of Pd-based bimetallic nanocluster catalysts

The N-C support was synthesized through the molten salt (ZnCl_2) method with hexaketocyclohexane and urea as precursors [42]. The prepared N-C support possessed a large BET surface area of $990 \text{ m}^2 \text{ g}^{-1}$ and hierarchically porous structures with both micropores and mesopores, as revealed by the nitrogen sorption analyses (Fig. S1). The nitrogen content of the N-C support was 11.7 wt%, as determined by elemental analysis; and negligible Zn species ($<0.1 \text{ wt}\%$) left according to the ICP-AES measurement. XPS analyses showed that the nitrogen content (13.2 wt%) was slightly higher than the result of elemental analysis (Figure S2). The high-resolution N 1s spectra of N-C show four typical bonding configurations of N atoms, including pyridinic (398.3 eV, 44.5%), pyrrole (399.8 eV, 18.7%) graphitic (400.6 eV, 34.3%) and oxidized (O-C, 402.2 eV, 2.5%) nitrogen.

Pd-based bimetallic catalysts were then prepared via a conventional impregnation method that involved the wet-impregnation of common metal salt precursors onto the N-C supports and subsequent high-temperature H_2 -reduction at 400~500 °C (**Fig. 1**). We totally synthesized 9 Pd-based bimetallic nanoclusters on N-C, including Pd alloyed with 2 noble metals (Pd-Ru, Pd-Rh) and 7 non-precious metals (Pd-Fe, Pd-Ga, Pd-Ge, Pd-Sn, Pd-Sb, Pd-Pb, and Pd-Bi). The total metal loading of the catalysts was in the range of 4.8-12.3 wt%. The detailed synthesis recipes of the catalysts were summarized in

Table S1.

The morphologies of the catalysts were first analyzed by the HAADF-STEM. We observed numerous tiny (<2 nm) nanoparticles that were homogeneously distributed throughout the N-C supports with narrow size distribution for all the samples (**Fig. 2** and Fig. S3). The average particle sizes of the bimetallic nanoclusters were estimated to be in the range of 0.9~1.8 nm, according to the statistical results for more than 200 randomly selected particles (inserts in **Fig. 2**). Powder XRD patterns present no or very broad diffraction peaks associated with metal species at 35-45° 2 θ (Fig. S4), indicating the absence of large particles on the N-C support. The broad peak at around 26° 2 θ is assigned to the N-C support with low graphitization degree. EDS element-mapping measurements were then carried out to image directly the elemental distribution in individual particles. The overlap of Pd and the second metal maps (Ru, Rh and Pb) in individual particles clearly demonstrates the homogeneous solid solution structure of the bimetallic nanoclusters without phase separation (**Fig. 3a-c**). EDS line scan tests additionally verified the homogeneous distribution of Pd and the second metal element in individual nanoclusters for other 6 bimetallic catalysts (**Fig. 3d** and Figure S5). Atomic-resolution HAADF-STEM measurements revealed that the Pd-Pb bimetallic clusters were crystalline and that some metal single atoms co-existed in Pd-Pb/N-C (**Fig. 3e**).

To experimentally identify the crucial role of nitrogen-fixing on the formation of ultrasmall bimetallic nanoclusters on N-C, we carried out several control syntheses with reference carbon supports. First, we removed most doped nitrogen atoms from the support by annealing the pristine N-C at a high temperature of 1100 °C under H₂/Ar atmosphere to obtain the LN-C. The nitrogen content was sharply decreased to 1.4 wt% after the denitrification process, while the specific surface area and porous structure were well sustained (Fig. S1 and Table S2). In addition, porous oxygen-doped carbon

(O-C) with a BET surface area of $1646 \text{ m}^2 \text{ g}^{-1}$ was also synthesized with the same molten salt method by replacing the hexaketocyclohexane and urea precursors with glucose. We then compared the fixing ability of the N-C, LN-C, O-C, and commercial carbon black Ketjenblack EC-600JD (K-600J, BET surface area of $1382 \text{ m}^2 \text{ g}^{-1}$) supports for monometallic Pd nanoparticles under H_2/Ar atmosphere at $500 \text{ }^\circ\text{C}$. As demonstrated in Fig. S6a, Pd nanoparticles were homogeneously dispersed on N-C with an average size of 2.7 nm without large particle or serious agglomeration. In contrast, we observed larger Pd particles on the LN-C (4.4 nm), O-C (4.6 nm) and K-600J (4.4 nm) supports, accompanied with a broad particle size distribution (Fig. S6b-d). The much broader peaks in XRD pattern for Pd/N-C compared to Pd/LN-C, Pd /O-C and Pd/K-600J further verified the smaller Pd particles on N-C (Fig. S7). Similarly, for loading bimetallic Pd-Pb and Pd-Ga nanoparticles, the LN-C and K-600J supports also exhibited much inferior ability in suppressing the metal growth and aggregation (Fig. S8). These results definitely prove that the capability of N-C for anchoring ultrasmall nanoclusters is strongly associated with nitrogen-containing sites. Note that the particle size of bimetallic Pd-M ($0.9\sim 1.8$) is much smaller than that of monometallic Pd (2.7), indicating that the alloying could also suppress the agglomeration [43-45].

We then performed the XPS, X-ray absorption near-edge structure (XANES), and extended X-ray absorption fine structure (EXAFS) analyses of Pd/N-C and Pd/LN-C to identify the chemical interaction between Pd and N species in the N-C support. The peak at $\sim 398.3 \text{ eV}$ in the $\text{N}1\text{s}$ XPS spectra of Pd/N-C slightly shifted to lower energy side by 0.2 eV compared to that of pristine N-C support (**Fig. 4a**), which might be attributed to the coordination of Pd with pyridinic N, as the negative palladium complex ions (PdCl_4^{2-}) would be preferentially attracted by protonated pyridinic N atoms in the acid solution via the electrostatic interaction [46]. The Pd 3d XPS spectra indicated that most of

Pd species in Pd/N-C were in oxidized state (**Fig. 4b**), which can be ascribed to the small-size effect [47] or the strong chemical interaction between Pd and nitrogen [48]. Differently, the Pd species in Pd/LN-C were mainly in metallic state due to the much larger Pd particles and the lack of Pd-N interaction. The intensity of white line of Pd species in the XANES of Pd/N-C was slightly higher than that of Pd foil and Pd/LN-C and much lower than that of PdO (**Fig. 4c**), demonstrating that the Pd species were partial oxidized, which is consistent with the XPS results. In the Fourier-transformed (FT) K^2 -weighted EXAFS spectra, the main peak at $\sim 2.55 \text{ \AA}$ in Pd/N-C and Pd/LN-C were ascribed to Pd-Pd bond (**Fig. 4d**). Compared with Pd foil, a new distinct peak appeared at $\sim 1.48 \text{ \AA}$ (slightly lower than Pd-O bond in PdO) for the Pd/N-C, which could be attributed to Pd-N or Pd-C coordination. Additionally, a relative weak peak at the same position was observed on Pd/LN-C due to the much lower coordinated N species in LN-C.

Overall, the above spectroscopic studies strongly imply the presence of strong chemical interaction between Pd and the N-C supports, which plays the pivotal role in fixing ultrasmall bimetallic nanoclusters.

3.2. Catalytic performance investigation

To demonstrate the utility of the bimetallic nanocluster catalysts, we studied the catalytic properties of Pd-Pb/N-C for the semihydrogenation of phenylacetylene. Semihydrogenation of alkynes to alkenes is of tremendous importance in polymer industry and academia [49-52], as a trace of alkynes in the alkene feed stream will seriously poison the catalysts used for the polymerization process. One of the most simple and practical methods for removing the alkyne poisons is the semihydrogenation of alkynes to alkenes with high selectivity. By alloying Pd metal with Pb, the hydrogenation of C=C bond

could be well blocked via rational poisoning the active sites, resulting a selectivity for the semihydrogenation of alkynes to alkenes [53, 54].

The semihydrogenation of phenylacetylene was conducted in an autoclave reactor under a mild environment (30 °C, 5 bar H₂). Two N-C supported bimetallic Pd-Pb nanocluster catalysts with Pd/Pb mole ratio of 1:1 and 1:2 were tested. K-600J supported Pd-Pb nanoparticles with Pd/Pb mole ratio of 1:2 were also tested for comparison. As shown in **Fig. 5a**, nearly 100% conversion of phenylacetylene was obtained in 90 minutes with a high styrene selectivity of > 93% for the bimetallic Pd-Pb/N-C (Pd/Pb=2:1) catalyst. Moreover, only a slight decline of selectivity by ~1% was observed when the reaction time was prolonged to 120 minutes. Although the increase of the Pd/Pb ratio to 1:1 could improve the activity for the Pd-Pb alloy catalysts with a high phenylacetylene conversion of > 98% achieved in only 60 minutes, the selectivity for styrene declined rapidly to around 80% when prolonging the reaction time to another 30 minutes (**Fig. S9a**). These results indicate that the overhydrogenation of C=C bond could not be effectively suppressed with a relative low Pb ratio in Pd-Pb/N-C, which is similar to the reported works [55, 56]. While for the Pd-Pb/K-600J catalyst, less than 40% conversion was got in 120 minutes under the same condition (**Fig. 5b**). The much lower activity of Pd-Pb/KEC-600J should be associated with their low metal utilization as a result of the inhomogeneous particle size distribution (see **Fig. S8c**). To further evaluate the activity of the catalysts, turnover frequencies (TOFs) were calculated under the phenylacetylene conversion in the range of 15~30% to ensure that the reaction remained under kinetic control. The TOF for the phenylacetylene semihydrogenation over Pd-Pb/N-C (Pd/Pb=1:2) was as high as 1092 hour⁻¹ based on the total amount of Pd (**Fig. 5c**), which is almost 3 times higher than that of Pd-Pb/K-600J (TOF = 280 hour⁻¹). Additionally, the activity of Pd-Pb/N-C (Pd/Pb=1:2) was also much higher (2~50 times) than that of

reported monometallic Pd [57] and Au catalysts [51, 58, 59] and bimetallic Pd-Pb [54, 60] catalysts. The detailed comparison of the performance of recently reported catalysts for selectively catalyzing alkynes were summarized in Table S3. Although the commercial Pd/C (5 wt%) catalysts has a very high TOF of 4518 hour^{-1} , a sharply decreased selectivity towards styrene was observed at high (> 99%) phenylacetylene conversion (Fig. S9b).

We contribute the high selectivity of Pd-Pb/N-C toward styrene to the alloying effects and small size (< 2 nm) effects. Alloying Pd with Pb could induce downshift of Pd d-band at the fermi level, which in turn significantly reduce the adsorption energy of C=C bond [61, 62]. The weaker adsorption ability of Pd-Pb alloy for C=C bond might lead to a fast desorption rate of styrene from the alloy surface and thus effectively suppress the over-hydrogenation of styrene. Moreover, the embedding of Pb atoms into the Pd crystal lattice and small particle size could prevent the formation of highly active (have no selectivity) subsurface β -PdH species [54, 63], which also could inhibit the over-hydrogenation process [64].

The stability of the Pd-Pb/N-C (Pd/Pb=1:2) catalyst was then established by intermittent cyclic tests under a partial conversion of around 80%. After five cycle runs, the phenylacetylene conversion were well sustained in the range of 78-80%, with an almost unchanged selectivity of >96% to styrene (**Fig. 5d**). No aggregation of Pd-Pb alloy was observed by HAADF-STEM after cyclic tests (Fig. S10), demonstrating the high stability of Pd-Pb alloys on N-C when catalyzing the alkyne semihydrogenation. Furthermore, the superior chemoselective hydrogenation properties could also be generalized to diverse terminal alkynes (Table 1), including aromatic and linear alkynes with various functional groups, including halogen, alkyl, hydroxyl, and carboxyl.

4. Conclusion

In summary, we have demonstrated a universal nitrogen-fixing strategy for producing a family of sub-2 nm Pd-based bimetallic nanocluster catalysts. Our methodology is based on the strong chemical interaction between metals and the N-C supports, which significantly suppresses metal aggregation during the H₂-reduction at an evaluated temperature and ensures the formation of bimetallic nanoclusters. The as-prepared bimetallic Pd-Pb catalyst showed a 3-fold higher activity than the carbon black supported Pd-Pb nanoparticle catalyst for the semihydrogenation of phenylacetylene, and sustained a high selectivity of >90 % under full conversion. The synthetic capability of our method would enable a comprehensively exploring of the application potentials of bimetallic nanocluster catalysts in diverse important reactions.

Author Contributions

H.-W.L. and L.W. conceived and designed the experiments. L.W., P.Y., S.-C. S, and S.-L.X synthesized and characterized the catalysts. L.-L.Z. performed the nitrogen sorption tests. P.C. performed the XPS measurements. L.W. and H.-W.L. co-wrote the manuscript. All authors discussed the results and commented on the manuscript.

Conflict of interest

The authors declare no competing financial interest.

Acknowledgements

This work was supported by the National Key Research and Development Program of China (Grant 2018YFA0702001), the National Natural Science Foundation of China (Grant 21671184), the Fundamental Research Funds for the Central Universities (Grant WK2060190103), the Joint Funds from Hefei National Synchrotron Radiation Laboratory (Grant KY2060000107), and the Recruitment

Program of Thousand Youth Talents. We acknowledge Shanghai Synchrotron Radiation Facility (BL14W1 beam line) for the synchrotron beam time.

Appendix A. Supplementary data

Supplementary material related to this article can be found, in the online version, at <https://doi.org/>

References

- [1] H. Liu, T. Jiang, B. Han, S. Liang, Y. Zhou, *Science* 326 (2009) 1250-1252.
- [2] Y. Wang, J. Yao, H. Li, D. Su, M. Antonietti, *J. Am. Chem. Soc.* 133 (2011) 2362-2365.
- [3] S. Mao, B. Zhao, Z. Wang, Y. Gong, G. Lu, X. Ma, L. Yu, Y. Wang, *Green Chem.* 21 (2019) 4143-4151.
- [4] T. Xue, Z. Lin, C.-Y. Chiu, Y. Li, L. Ruan, G. Wang, Z. Zhao, C. Lee, X. Duan, Y. Huang, *Sci. Adv.* 3 (2017) e1600615.
- [5] T.L. Cui, W.Y. Ke, W.B. Zhang, H.H. Wang, X.H. Li, J.S. Chen, *Angew. Chem. Int. Ed.* 55 (2016) 9178-9182.
- [6] V. Mazumder, S. Sun, *J. Am. Chem. Soc.* 131 (2009) 4588-4589.
- [7] M. Luo, Z. Zhao, Y. Zhang, Y. Sun, Y. Xing, F. Lv, Y. Yang, X. Zhang, S. Hwang, Y. Qin, J.Y. Ma, F. Lin, D. Su, G. Lu, S. Guo, *Nature* 574 (2019) 81-85.
- [8] J.G. Firth, H.B. Holland, *Nature* 217 (1968) 1252-1253.
- [9] J. Xu, T. White, P. Li, C. He, J. Yu, W. Yuan, Y.-F. Han, *J. Am. Chem. Soc.* 132 (2010) 10398-10406.
- [10] L. Zhang, H. Liu, X. Huang, X. Sun, Z. Jiang, R. Schloegl, D. Su, *Angew. Chem. Int. Ed.* 54 (2015) 15823-15826.
- [11] A. McNally, B. Haffemayer, B.S.L. Collins, M.J. Gaunt, *Nature* 510 (2014) 129-133.
- [12] C.C.C.J. Seechurn, M.O. Kitching, T.J. Colacot, V. Snieckus, *Angew. Chem. Int. Ed.* 51 (2012) 5062-5085.
- [13] J. Park, S. Hong, *Chem. Soc. Rev.* 41 (2012) 6931-6943.
- [14] J. Osswald, K. Kovnir, M. Armbruster, R. Giedigkeit, R.E. Jentoft, U. Wild, Y. Grin, R. Schloegl, *J. Catal.* 258 (2008) 219-227.
- [15] M. Armbruster, G. Wowsnick, M. Friedrich, M. Heggen, R. Cardoso-Gil, *J. Am. Chem. Soc.* 133 (2011) 9112-9118.
- [16] H. Zhang, M.S. Jin, Y.N. Xia, *Chem. Soc. Rev.* 41 (2012) 8035-8049.
- [17] M. Sankar, N. Dimitratos, P.J. Miedziak, P.P. Wells, C.J. Kiely, G.J. Hutchings, *Chem. Soc. Rev.* 41 (2012) 8099-8139.
- [18] K.D. Gilroy, A. Ruditskiy, H.-C. Peng, D. Qin, Y. Xia, *Chem. Rev.* 116 (2016) 10414-10472.
- [19] P. Claus, A. Brückner, C. Mohr, H. Hofmeister, *J. Am. Chem. Soc.* 122 (2000) 11430-11439.
- [20] N. Satoh, T. Nakashima, K. Kamikura, K. Yamamoto, *Nat. Nanotechnol.* 3 (2008) 106-111.
- [21] O. Lopez-Acevedo, K.A. Kacprzak, J. Akola, H. Häkkinen, *Nat. Chem.* 2 (2010) 329-334.
- [22] W. Zhu, Z. Wu, G.S. Foo, X. Gao, M. Zhou, B. Liu, G.M. Veith, P. Wu, K.L. Browning, H.N. Lee, H. Li, S. Dai, H. Zhu, *Nat. Commun.* 8 (2017) 15291.

- [23] R. Levy, N.T.K. Thanh, R.C. Doty, I. Hussain, R.J. Nichols, D.J. Schiffrin, M. Brust, D.G. Fernig, *J. Am. Chem. Soc.* 126 (2004) 10076-10084.
- [24] N. Wang, Q. Sun, J. Yu, *Adv. Mater.* 31 (2019) 1803966
- [25] Q. Sun, N. Wang, Q. Bing, R. Si, J. Liu, R. Bai, P. Zhang, M. Jia, J. Yu, *Chem* 3 (2017) 477-493.
- [26] F. Chen, K. Shen, J. Chen, X. Yang, J. Cui, Y. Li, *Acs Central Sci.* 5 (2019) 176-185.
- [27] X. Gu, Z.-H. Lu, H.-L. Jiang, T. Akita, Q. Xu, *J. Am. Chem. Soc.* 133 (2011) 11822-11825.
- [28] H.-L. Jiang, T. Akita, T. Ishida, M. Haruta, Q. Xu, *J. Am. Chem. Soc.* 133 (2011) 1304-1306.
- [29] M.S. El-Shall, V. Abdelsayed, A.E.R.S. Khder, H.M.A. Hassan, H.M. El-Kaderi, T.E. Reich, *J. Mater. Chem.* 19 (2009) 7625-7631.
- [30] A.S. Fung, M.J. Kelley, D.C. Koningsberger, B.C. Gates, *J. Am. Chem. Soc.* 119 (1997) 5877-5887.
- [31] S. Chotisuwan, J. Wittayakun, B.C. Gates, *J. Phys. Chem. B* 110 (2006) 12459-12469.
- [32] B. Liu, H. Yao, W. Song, L. Jin, I.M. Mosa, J.F. Rusling, S.L. Suib, J. He, *J. Am. Chem. Soc.* 138 (2016) 4718-4721.
- [33] X. Yang, J.-K. Sun, M. Kitta, H. Pang, Q. Xu, *Nat. Catal.* 1 (2018) 214-220.
- [34] Z. Niu, Y. Li, *Chem. Mat.* 26 (2014) 72-83.
- [35] O.S. Alexeev, B.C. Gates, *Ind. Eng. Chem. Res.* 42 (2003) 1571-1587.
- [36] A. Wong, Q. Liu, S. Griffin, A. Nicholls, J.R. Regalbuto, *Science* 358 (2017) 1427-1430.
- [37] K. Ding, D.A. Cullen, L. Zhang, Z. Cao, A.D. Roy, I.N. Ivanov, D. Cao, *Science* 362 (2018) 560-564.
- [38] N. Cheng, S. Stambula, D. Wang, M.N. Banis, J. Liu, A. Riese, B. Xiao, R. Li, T.-K. Sham, L.-M. Liu, *Nat. Commun.* 7 (2016) 13638.
- [39] H. Su, P. Gao, M.-Y. Wang, G.-Y. Zhai, J.-J. Zhang, T.-J. Zhao, J. Su, M. Antonietti, X.-H. Li, J.-S. Chen, *Angew. Chem. Int. Ed.* 57 (2018) 15194-15198.
- [40] C.H. Choi, M. Kim, H.C. Kwon, S.J. Cho, S. Yun, H.T. Kim, K.J.J. Mayrhofer, H. Kim, M. Choi, *Nat. Commun.* 7 (2016) 10922.
- [41] L. Wang, M.-X. Chen, Q.-Q. Yan, S.-L. Xu, S.-Q. Chu, P. Chen, Y. Lin, H.-W. Liang, *Sci. Adv.* 5 (2019) eaax6322.
- [42] N. Fechner, N.P. Zussblatt, R. Rothe, R. Schloegl, M.-G. Willinger, B.F. Chmelka, M. Antonietti, *Adv. Mater.* 28 (2016) 1287-1294.
- [43] C.W. Han, P. Majumdar, E.E. Marinero, A. Aguilar-Tapia, R. Zanella, J. Greeley, V. Ortalan, *Nano Lett.* 15 (2015) 8141-8147.
- [44] A. Cao, G. Vesper, *Nat. Mater.* 9 (2010) 75-81.
- [45] J. Zhang, Y. Deng, X. Cai, Y. Chen, M. Peng, Z. Jia, Z. Jiang, P. Ren, S. Yao, J. Xie, D. Xiao, X. Wen, N. Wang, H. Liu, D. Ma, *ACS Catal.* 9 (2019) 5998-6005.
- [46] Z. Zhang, Y. Chen, L. Zhou, C. Chen, Z. Han, B. Zhang, Q. Wu, L. Yang, L. Du, Y. Bu, P. Wang, X. Wang, H. Yang, Z. Hu, *Nat. Commun.* 10 (2019) 1657.
- [47] Y.T. Kim, T. Mitani, *J. Catal.* 238 (2006) 394-401.
- [48] Z. Li, X. Yang, N. Tsumori, Z. Liu, Y. Himeda, T. Autrey, Q. Xu, *ACS Catal.* 7 (2017) 2720-2724.
- [49] F. Studt, F. Abild-Pedersen, T. Bligaard, R.Z. Sørensen, C.H. Christensen, J.K. Nørskov, *Science* 320 (2008) 1320.
- [50] C.W. Chan, A.H. Mahadi, M.M. Li, E.C. Corbos, C. Tang, G. Jones, W.C. Kuo, J. Cookson,

- C.M. Brown, P.T. Bishop, S.C. Tsang, *Nat. Commun.* 5 (2014) 5787.
- [51] T. Mitsudome, M. Yamamoto, Z. Maeno, T. Mizugaki, K. Jitsukawa, K. Kaneda, *J. Am. Chem. Soc.* 137 (2015) 13452-13455.
- [52] D. Albani, M. Shahrokhi, Z. Chen, S. Mitchell, R. Hauert, N. Lopez, J. Perez-Ramirez, *Nat. Commun.* 9 (2018) 2634.
- [53] S. Furukawa, Y. Yoshida, T. Komatsu, *ACS Catal.* 4 (2014) 1441-1450.
- [54] W. Niu, Y. Gao, W. Zhang, N. Yan, X. Lu, *Angew. Chem. Int. Ed.* 54 (2015) 8271-8274.
- [55] P. Weerachawanasak, O. Mekasuwandumrong, M. Arai, S.-I. Fujita, P. Praserthdam, J. Panpranot, *J. Catal.* 262 (2009) 199-205.
- [56] L. Shen, S. Mao, J. Li, M. Li, P. Chen, H. Li, Z. Chen, Y. Wang, *J. Catal.* 350 (2017) 13-20.
- [57] Y. Kuwahara, H. Kango, H. Yamashita, *ACS Catal.* 9 (2019) 1993-2006.
- [58] G. Li, R. Jin, *J. Am. Chem. Soc.* 136 (2014) 11347-11354.
- [59] L. Shao, X. Huang, D. Teschner, W. Zhang, *ACS Catal.* 4 (2014) 2369-2373.
- [60] J. Zhang, W. Xu, L. Xu, Q. Shao, X. Huang, *Chem. Mat.* 30 (2018) 6338-6345.
- [61] G. Wowsnick, D. Teschner, M. Armbruester, I. Kasatkin, F. Girgsdies, Y. Grin, R. Schloegl, M. Behrens, *J. Catal.* 309 (2014) 221-230.
- [62] M. Armbruester, K. Kovnir, M. Behrens, D. Teschner, Y. Grin, R. Schloegl, *J. Am. Chem. Soc.* 132 (2010) 14745-14747.
- [63] D. Teschner, J. Borsodi, A. Wootsch, Z. Revay, M. Haevecker, A. Knop-Gericke, S.D. Jackson, R. Schloegl, *Science* 320 (2008) 86-89.
- [64] B. Coq, F. Figueras, *J. Mol. Catal. A-Chem.* 173 (2001) 117-134.

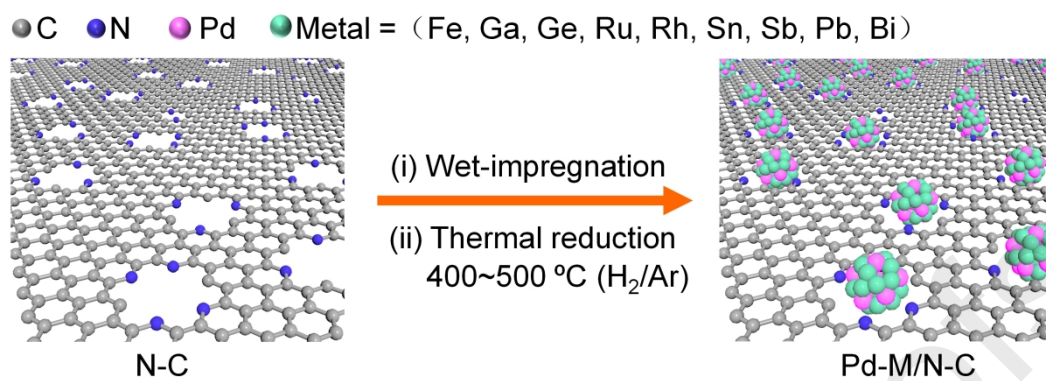


Fig. 1. Schematic illustration of the synthesis of carbon supported sub-2 nm Pd-based bimetallic nanoclusters by the nitrogen-fixing strategy.

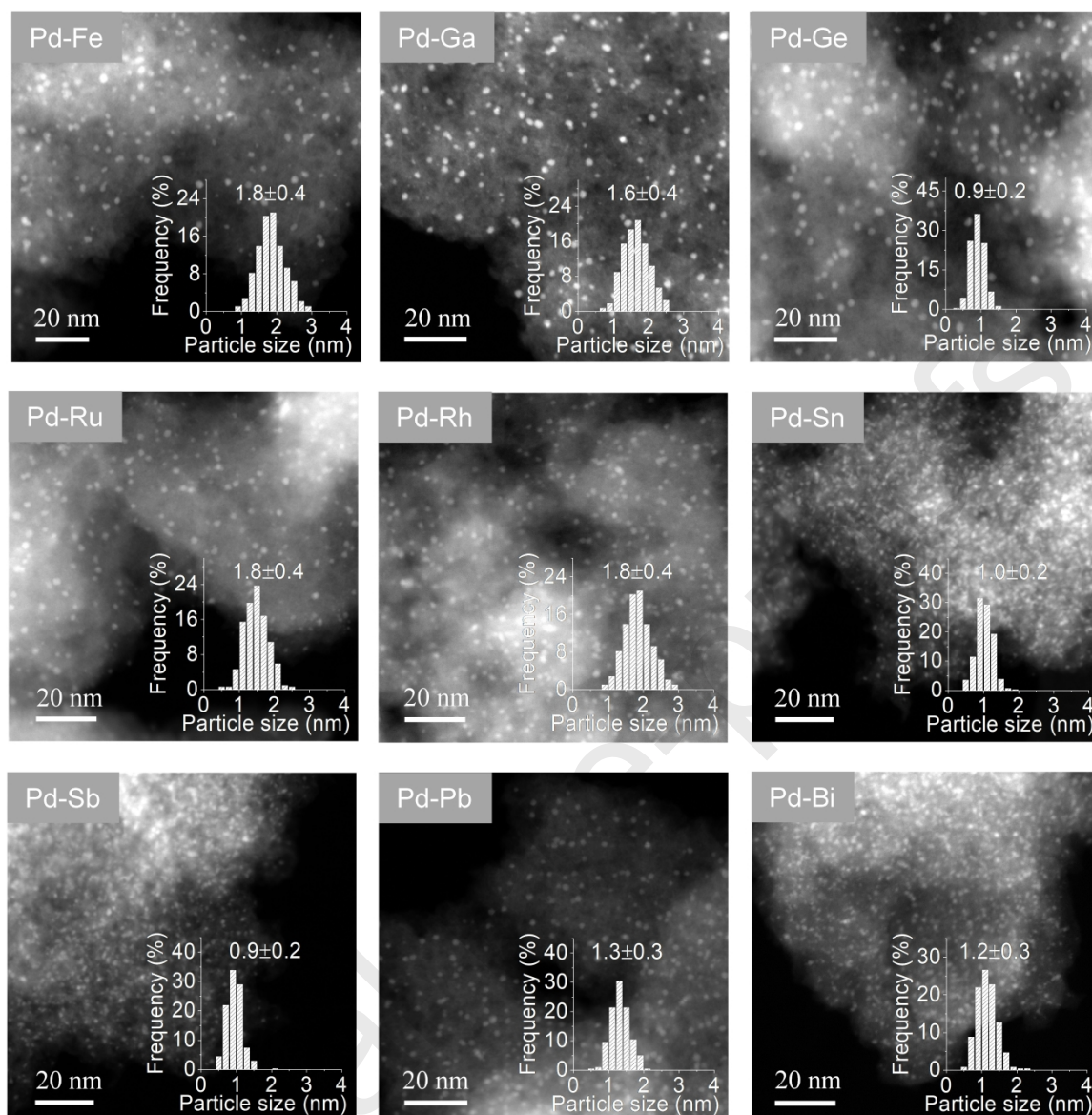


Fig. 2. HAADF-STEM images of 9 different N-C supported Pd-based bimetallic nanoclusters. Insets are the corresponding particle size distribution histograms.

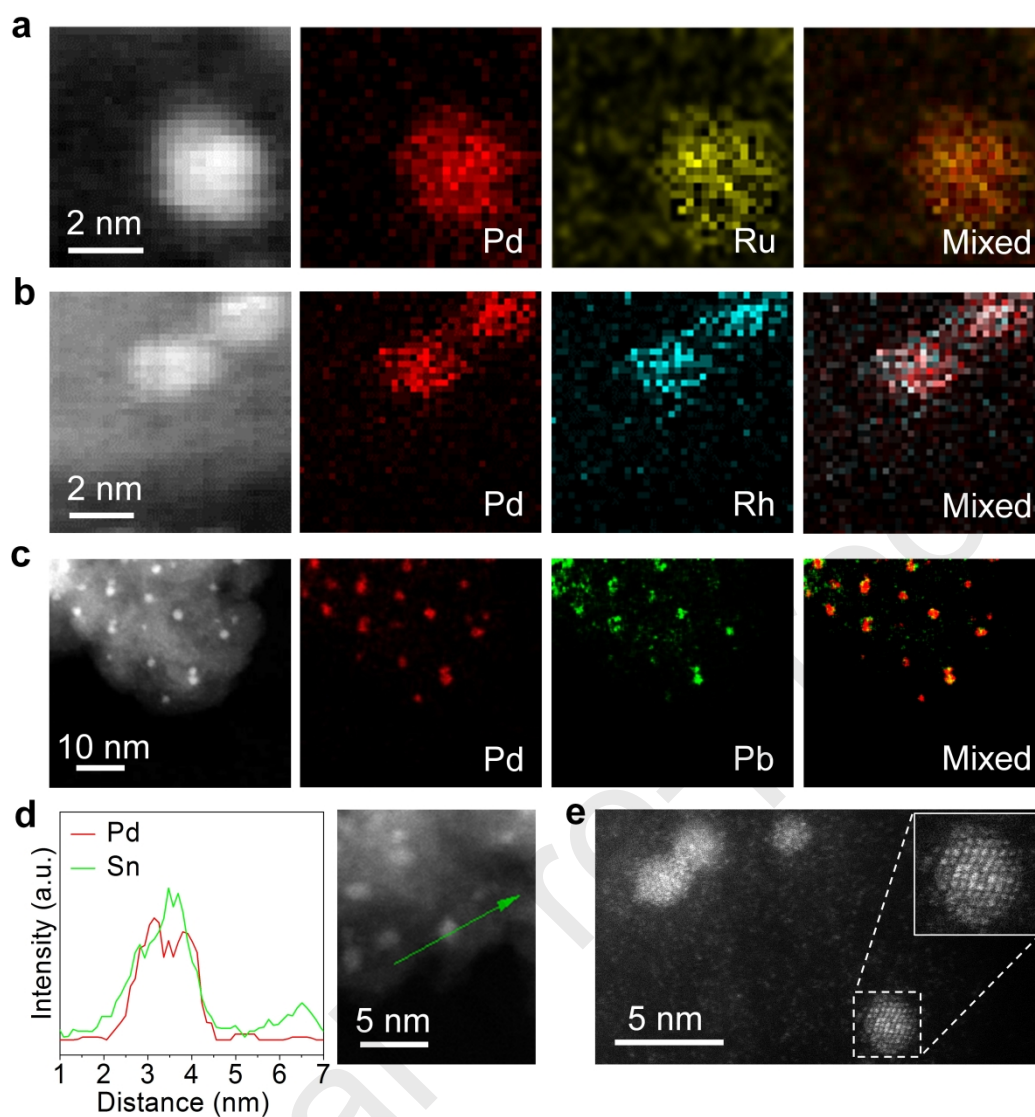


Fig. 3. (a-c) EDS elemental mappings of Pd-Ru/N-C (a), Pd-Rh/N-C(b), and Pd-Pb/N-C (c). (d) STEM-EDS line scan of Pd-Sn/N-C. (e) Atomic-resolution HAADF-STEM images of Pd-Pb/N-C.

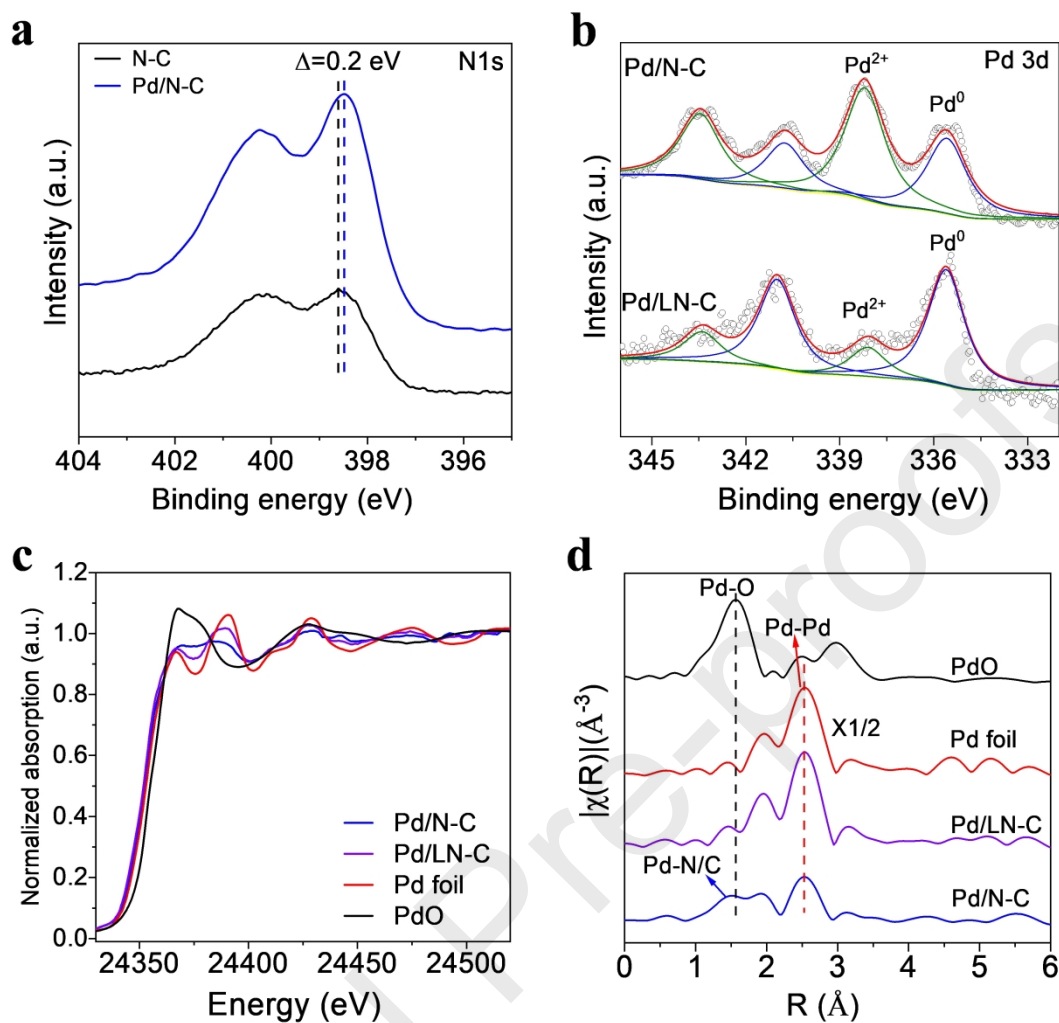


Fig. 4. (a) XPS spectra of N1s in N-C and Pd/N-C. (b) XPS spectra of Pd 3d in Pd/N-C and Pd/LN-C. (c) Normalized XANES spectra at the Pd *K*-edge and (d) the K^2 -weighted Fourier transform spectra of Pd/N-C, Pd/LN-C, Pd foil, and PdO.

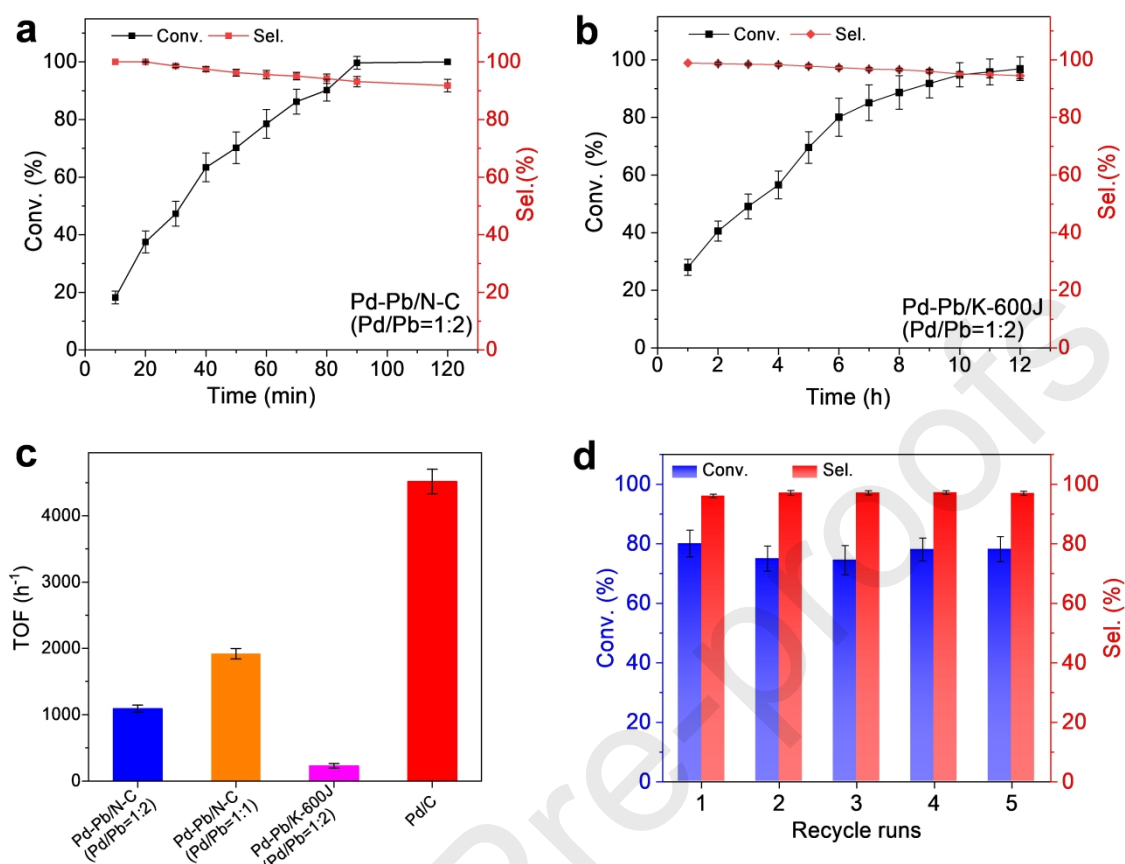
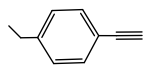
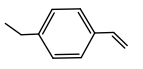
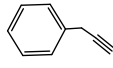
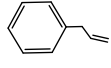
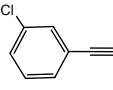
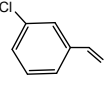
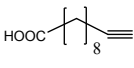
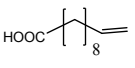
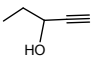
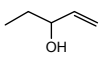
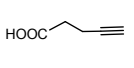
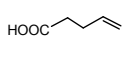
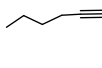
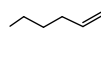
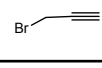
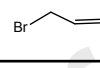


Fig. 5. (a-b) Catalytic performance for the phenylacetylene semihydrogenation over Pd-Pb/N-C (Pd/Pb=1:2) and Pd-Pb/K-600J, respectively. (c) TOF of Pd-Pb/N-C (Pd/Pb=1:2) and reference catalysts (based on the total Pd content). (d) Recycle of Pd-Pb/N-C (Pd/Pb=1:2) for the phenylacetylene semihydrogenation. React conditions: 1 mL ethanol, 1 mmol phenylacetylene, 0.1 at% Pd, 30 °C, 5 bar H₂.

Table 1. Semihydrogenation of terminal alkynes on the Pd-Pb/N-C (Pd/Pb=1:2) catalyst.

Entry	Substrate	Product	Conv. (%)	Sel. (%)
1			>99%	93.9
2			>99%	92.9
3			>99%	92.1
4			>99%	97.0
5			>99%	99.9
6			>99%	95.0
7			>99%	96.5
8			>99%	99.9

React conditions: 1 mL ethanol, 1 mmol substrate, 0.1 at% Pd, 2 h, 30 °C, 5 bar H₂.

Declaration of interests

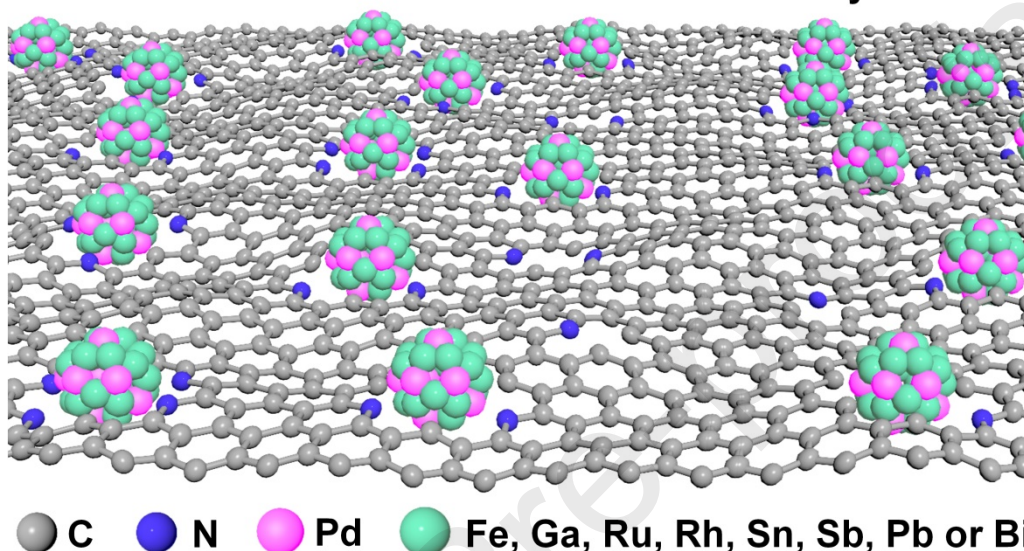
The authors declare that they have no known competing financial interests or personal relationships that could have appeared to influence the work reported in this paper.

The authors declare the following financial interests/personal relationships which may be considered as potential competing interests:

Journal Pre-proofs

Graphical Abstract

Pd-Based Bimetallic Nanoclusters Fixed by N-C



Ultrasmall Pd-based bimetallic nanoclusters were successfully synthesized on N-C support via a nitrogen-fixing strategy.

Highlights

- 9 **Pd-based bimetallic nanoclusters** were prepared by nitrogen-fixing strategy.
- **Strong metal-N interaction greatly suppresses the metal aggregation.**
- Pd-Pb/N-C display high catalytic performance for the semihydrogenation of alkynes.

Journal Pre-proofs